Infragravity waves in the deep ocean: An upward revision

J. Aucan[1] and F. Ardhuin[2]

Received 12 February 2013; revised 2 March 2013; accepted 5 March 2013.

[1] Ocean infragravity waves are surface gravity waves with periods of several minutes and corresponding wavelengths of up to tens of kilometers. When propagating freely in the deep ocean, these waves are typically small, several centimeters at most, so they have been seldom studied. In the context of future wide-swath altimetry missions, these waves need to be better quantified as they have wavelengths that will be resolved by such instruments. Here, we analyze the global climatology and variability of infragravity waves in the deep ocean using data from over 40 open ocean locations, with depths larger than 2000 m. We show that typical infragravity wave heights are higher than previously estimated, with winter-averaged values up to 11 mm off the U.S. West Coast, and typically less than 6 mm in the tropics. The mid to high latitudes exhibit a strong seasonal cycle consistent with the local variability of the wind-waves, while the tropical Pacific has a higher energy level during the Austral winter that does not correlate well with the local wind-waves, suggesting a remote source for the recorded infragravity waves. These infragravity wave energies are expected to be a significant contribution to the error budget for possible measurements of sea level associated to sub-mesoscale currents at horizontal scales around 10 km. Hence, a global numerical model of infragravity waves will likely be necessary for the analysis of the planned Surface Water Ocean Topography mission. **Citation:** Aucan, J., and F. Ardhuin (2013), Infragravity waves in the deep ocean: An upward revision, *Geophys. Res. Lett.*, *40*, doi:10.1002/grl.50321.

1. Introduction

[2] Wind-generated surface gravity waves are ubiquitous at the ocean surface. Their dominant period typically varies between 2 and 25 s, with a corresponding wavelength between 6 and 940 m. These wind-waves can be further separated into seas and swells according to the strong or negligible influence of the local wind on their evolution, but we shall call all these wind-waves. Longer and lower frequency surface gravity waves, called infragravity (IG) waves, are generated by the nonlinear interactions of the wind-waves and have dominant periods comprised between 1 and 10 min. IG waves either appear as "free" [*Herbers et al.*, 1994] or "bound" [*Herbers et al.*, 1995].

[3] Bound IG waves are determined by the local wind-waves and do not follow the dispersion relationship of linear surface gravity waves. They have much shorter wavelengths that are the length of the local wind-wave groups. The spectrum of these bound IG waves can be estimated accurately from the measured spectrum of the wind-waves [*Herbers et al.*, 1994]. This wind-wave spectrum can also be estimated by numerical wind-wave models. Bound IG waves are released and become free at the shoreline where the wind-waves break.

[4] Free IG waves, on the other hand, disperse like linear surface gravity waves. The shoreline boundary condition imposes their frequency to match that of the bound waves, so that the free IG waves have horizontal wavelengths up to tens of kilometers in deep water. The liberation of bound IG into free IG at the shoreline is now relatively well understood [e.g., *Henderson and Bowen*, 2003] but remains a difficult modeling problem. Given their long wavelength, most of the outbound free IG energy is trapped by refraction on the shelf, and only a small fraction of the IG energy leaks into the open ocean as free waves [e.g., *Webb et al.*, 1991]. The amount of leaky infragravity radiated offshore for a given incident short wave spectrum on a given coastline is poorly documented, and likely depends on multiple parameters. As a result, little is known about typical energy levels and variability of free infragravity energy in the open ocean. Despite this poor knowledge, open ocean infragravity have been linked to other geophysical processes such as ice-shelf breaking [*Bromirski et al.*, 2010] and the generation of global seismic noise [*Webb*, 2008]. Remotely generated free IG waves can also be observed at coastlines, in addition to locally generated IG waves [*Harmon et al.*, 2012]. More importantly, and despite their small amplitude, free IG waves in the open ocean may still be high enough to be measured by the future Ka-band radar interferometer on board the Surface Water and Ocean Topography mission [SWOT, see *Alsdorf et al.*, 2007]. The temporal and spatial variability of IG waves needs to be determined and understood in this context. In this study, we use long records of high-frequency bottom pressure from the Deep ocean Assessment and Reporting of Tsunami (DART) program and other programs to document the open ocean temporal and spatial variability of free IG wave energy in both the Pacific and Atlantic Ocean.

2. Data Preparation

[5] The DART stations are typically composed of a bottom package and a nearby surface buoy. The bottom package holds a Bottom Pressure Recorder (BPR), which performs one measurement every 15 s, and some of the data are trans-

[1]Institut de Recherche pour le Développement (IRD) Laboratoire d'Etudes en Géophysique et Océanographie Spatiale (LEGOS), Toulouse University (UPS), Toulouse, France.
[2]Ifremer, Laboratoire d'Oceanographie Spatiale et Laboratoire de Physique et Dynamique Sedimentaire, Brest, France.

Corresponding author: J. AUCAN, Institut de Recherche pour le Développement (IRD) Laboratoire d'Etudes en Géophysique et Océanographie Spatiale (LEGOS), Toulouse University (UPS), Toulouse, France. (jerome.aucan@ird.fr)

0094-8276/13/10.1002/grl.50321

mitted acoustically to the surface buoy, which transmits it to land via satellite links. Because of the communication costs, the full resolution data are only transmitted during suspected tsunami events. It is only every 1 to 2 years that the BPR is brought back up to the surface for servicing, and the continuous full resolution pressure record becomes available. These records were obtained from the U.S. National Geophysical Data Center and the Australian Bureau of Meteorology. Additional data were obtained from two BPR deployed between September 2008 and September 2009 at the Mid-Atlantic Ridge research site "Lucky Strike", courtesy of V. Ballu (Institut de Physique du Globe de Paris; IPGP), and from the North Pacific Barometric Electromagnetic and Pressure Experiment (1986–1987), courtesy of D. Luther (School of Ocean and Earth Science and Technology). At some stations, the continuous pressure records span several years. In total, we have analyzed records from 40 locations in the Pacific and Atlantic Oceans, with depths ranging from 3 to 6 km. Because their wavelengths are typically shorter than these depths, the pressure signal at the seafloor from both wind-waves and most bound IG components is strongly attenuated from its surface value and thus overwhelmed by the free IG signal [*Webb et al.*, 1991]. We therefore assume that the pressure signal over the frequency band of interest (1–20 min) that we observe at all the stations are solely due to freely propagating infragravity waves, that satisfy the surface gravity wave dispersion. For a free monochromatic wave of wavenumber k, the bottom amplitude of pressure p_b is related to the surface elevation amplitude a, by a transfer function M that is a function of the water depth D

$$p_b = aM = a\frac{\rho g}{\cosh(kD)}, \tag{1}$$

where ρ is the water density, g is gravity acceleration. The wavenumber, k, is related to the wave frequency f by the dispersion relation [*de Laplace*, 1776], $(2\pi f)^2 = gk\tanh(kD)$. A Fourier analysis was performed on each day-long bottom pressure record to obtain the bottom pressure power spectral densities $F_p(f)$. The transfer function M (equation 1), is then applied to obtain the surface elevation spectral density $E(f)$,

$$E(f) = M^2 F_p(f). \tag{2}$$

[6] The average shape of the bottom pressure and inferred surface elevation spectra are shown in Figure 1. The pressure spectra transitions from an f^{-2} slope at frequencies below 0.002 Hz, to a nearly flat spectrum at higher frequencies, are consistent with earlier measurements [*Webb et al.*, 1991; *Filloux*, 1980]. This is followed by a sharp drop at frequency above 10^{-2} Hz, corresponding to the "noise notch" described by *Webb et al.* [1991] and *Filloux* [1980], which arises from the hydrodynamic filtering of free gravity waves at these depths, and the transition to frequencies dominated by acoustic modes (more precisely Rayleigh wave modes : *Ardhuin and Herbers* [2013]). The three-hourly energy levels at any pairs of frequencies between 0.0025 Hz and 0.012 Hz are well correlated ($r > 0.7$) and waves in this band have been shown to be consistent with the transformation of bound to free infragravity waves at the shoreline *Webb et al.* [1991]. If one of the two frequencies is taken below 0.0015 Hz, then the correlation is much smaller. Although the correlation should be reduced by dispersive propagation, it is also possible that pressure signals for $f < 0.002$ Hz are not caused by the transformation of bound to free infragravity waves at the shoreline but are more likely caused by atmospheric forcing. Indeed, *Luther et al.* [1990] and *de Jong et al.* [2003] have shown that pressure signals around 1 mHz were coherent with wind forcing and that winds could explain these signals. The significant IG wave height H_{IG} was defined from a partially integrated spectrum as,

$$H_{IG} = 4\sqrt{\int_{f_{min}}^{f_{max}} E(f)\mathrm{d}f}. \tag{3}$$

[7] We chose $f_{min} = 8.3\times10^{-4}$ Hz and $f_{max} = 1.1\times10^{-2}$ Hz, corresponding to 20 and 1.5 min periods, respectively. As a result, $M > 0.1$ at all stations, which removes the contribution of high frequency measurement noise to our estimate of H_{IG}. This common cut-off frequencies for all stations make H_{IG} estimates from different stations more readily comparable. Spurious peaks of H_{IG} were removed from the data set. These peaks are expected to be caused by tsunamis events, sensors malfunctions, or physical disturbances of the BPR. At each station, we calculate a background noise level $H_{IG,min}$ as the lowest 5% values of H_{IG}. This noise level is similar at all the stations considered in this study, all falling between 3 and 5 mm. At each station, we calculate $H_{IG,summer}$ and $H_{IG,winter}$ as the time-averaged H_{IG} during boreal summers and winters, respectively, as shown in Figure 1.

3. IG Seasonality and Spatial Distributions

[8] We used a total of 29 stations in the Pacific Ocean (Figure 2), six stations in the Atlantic Ocean (Figure 3), one station in the Gulf of Mexico, and one station in the Indian Ocean, off Australia. Seasonal variability in the spectra is more pronounced at frequencies between 10^{-3} and 10^{-2} Hz, as was already shown by *Filloux et al.* [1991] (Figure 1, top), and the corresponding wave height H_{IG} (Figure 1, bottom) expectedly shows a strong seasonality. Episodic events of elevated H_{IG}, of the order of a few days, are noticeable, with maximum values of H_{IG} reaching well over 2 cm (Figure 1, bottom).

[9] The observed spatial and temporal distribution of H_{IG} is consistent with an IG wave generation at nearby coastlines by strong winter storms (Figure 2). We find the highest values of H_{IG} and the strongest seasonality in the NE Pacific (Figure 2), where $H_{IG,winter}$ is up to factor 2 higher than $H_{IG,summer}$. H_{IG} appears to become smaller going westward in the North Pacific, probably related to increasing incident swell heights in the East and the convex shape of the Alaska peninsula and Aleutian Islands from which the IG free energy can disperse over a wider ocean region. *Filloux et al.* [1991] showed a predominant origin of IG waves to be in the British Columbia region. Our data are clearly consisted with that conclusion.

[10] In lower latitudes in the Pacific (Figure 2), H_{IG} becomes smaller and the seasonality less pronounced. Near the Equator in the Eastern Pacific and in the Southern Hemisphere, the seasonality is reversed, reflecting a predominant formation region of IG waves during boreal summer in the southern hemisphere.

[11] There are fewer stations available in the Atlantic ocean than in the Pacific ocean, and they are confined to the North-West Atlantic (Figure 3). From these, we can say that the Atlantic seasonality is similar to that of the Pacific. Also,

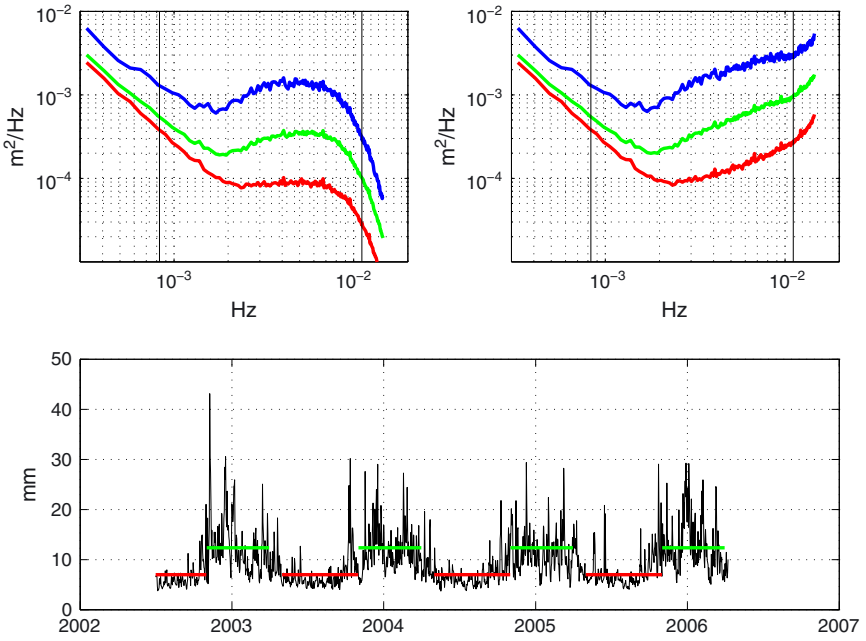

Figure 1. Example data from station 46405, off the U.S. Oregon coast; (top panel, left) Average observed bottom pressure spectra p_b and (top panel, right) surface corrected pressure spectra a, during the summer (red), the winter (green), and during the 5% highest events (blue). The black vertical lines represent the frequency limits f_{min} and f_{max} over which H_{IG} at all stations was calculated. (bottom panel) H_{IG} (black), averaged summer (winter) IG wave height $H_{IGsummer}$ ($H_{IGwinter}$) in red (green).

while *Webb et al.* [1991] reported that IG waves were less energetic in the Atlantic Ocean than in the Pacific, we do not see any clear difference between the U.S. East coast and the asian East coasts at the same latitude. We note that preliminary numerical modeling efforts, using parametric free IG sources along the coasts, suggest that the North-West Europe Shelf and passage between Iceland and Ireland is the largest source of free IG waves of the world ocean, but the model has to be refined before it can be trusted. Measurements off the European coasts will therefore be critical to verify this trend. Going back to *Webb et al.* [1991], who analyzed data from the HEBBLE site (Figure 3), he warned that the site may have been sheltered from IG waves by the Grand Banks. Other sites in the Pacific Ocean included in this study may experience similar sheltering, and as a result show low level of IG energy. These sites include DART 51407 West of Hawaii Island, and DART 51425 off Samoa. The numerical model of IG sources and propagation that is under development will be used to verify this sheltering effect.

4. Expected Wavenumber Spectra Along a Possible Altimeter Track

[12] In order to illustrate the estimated surface elevation contribution to satellite altimeter measurements, we have chosen one of the most energetic stations and converted the frequency spectrum to one-dimensional wavenumber spectrum. This was done by assuming that all IG spectra are isotropic. This is clearly not a realistic assumption, as shown by *Webb et al.* [1991], but it allows a simple analysis that does not require a choice of track orientation and should provide a useful order of magnitude estimate.

[13] For such an isotropic spectrum, the frequency-direction spectral density is $E(f,\theta) = E(f)/(2\pi)$. For linear waves, the wavenumber spectrum $E(k_x,k_y)$ is given by $E(k_x,k_y) = C_g E(f,\theta)/(2\pi k)$, where C_g is the group speed. These relations give

$$E(k_x,k_y) = \frac{f}{4\pi k^2}\left(1+\frac{2kD}{\sinh(2kD)}\right)E(f) \qquad (4)$$

and, taking a track along the x axis, we have a wavenumber spectrum,

$$E(k_x) = \int_{-\infty}^{+\infty} \frac{f}{4\pi k^2}\left(1+\frac{2kD}{\sinh(2kD)}\right)E(f)\mathrm{d}k_y. \qquad (5)$$

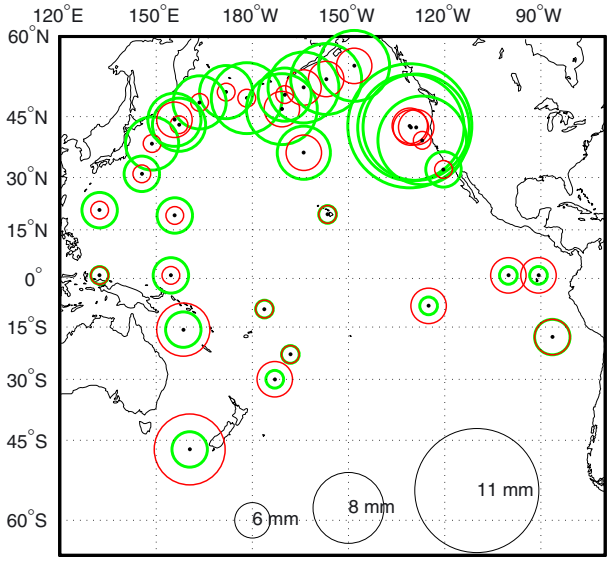

Figure 2. Mean summer (winter) infragravity wave height in red (green) represented by the size of each circle.

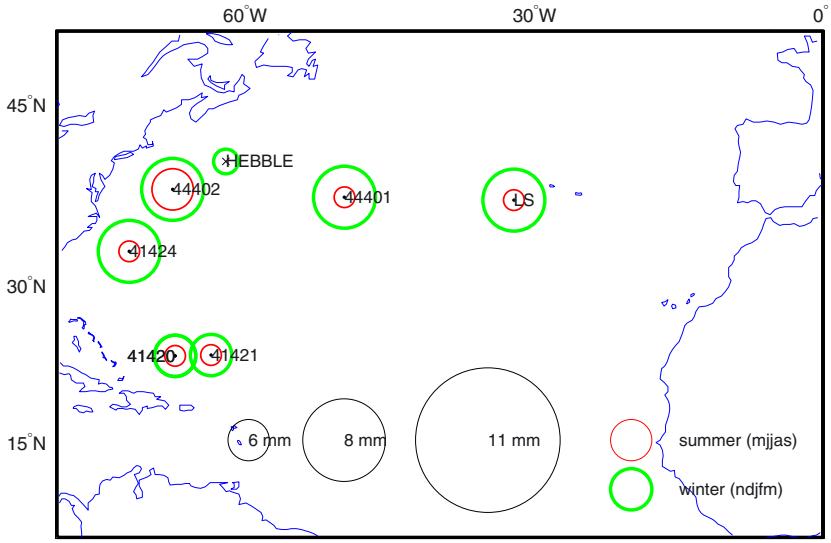

Figure 3. Mean summer (winter) wave height in red (green) represented by the size of each circle. Numbered stations correspond to DART stations. LS correspond to the Lucky Strike BPR data, courtesy of IPGP. HEBBLE is the site used in *Webb et al.* [1991], and a single value of 1.2 mm is assigned to the site based on his Figure 6a).

[14] We see that the shorter wavelengths that are propagating very obliquely compared to the track, with $k_y >> k_x$, can contribute significantly to the spectral level. However, given the rapid roll-off of $E(f)$ towards high frequencies, the $E(k_x)$ level is usually dominated by the components with $k_y < k_x$. Also, sea level measurements with a satellite altimeter also involve an average in the y direction which is not included here but could be easily represented by including in the integral a multiplication by the Fourier transform of the averaging kernel.

[15] At station 46405, the maximum frequency f_{max} = 0.01 Hz used in our integration to obtain H_{IG} corresponds to a minimum wavelength of 15 km. At that frequency and for a depth of 3600 m, a spectral level $E(f) = 0.002$ m^2/Hz yields an along-track spectral level $E(k_x) = 1$ cm^2/(cycle/km). This is twice the level expected for the submesoscale altimetric signal when using a $k^{-11/3}$ extension of the spectra shown by *Le Traon et al.* [2008] for the Gulf Stream, Agulhas, and Kuroshio regions, and of the order of the spectral level that may be extrapolated from less energetic regions *Xu and Fu* [2011]. This is also the initial mission requirement for the noise level for the Surface Water Ocean Topography (SWOT) mission.

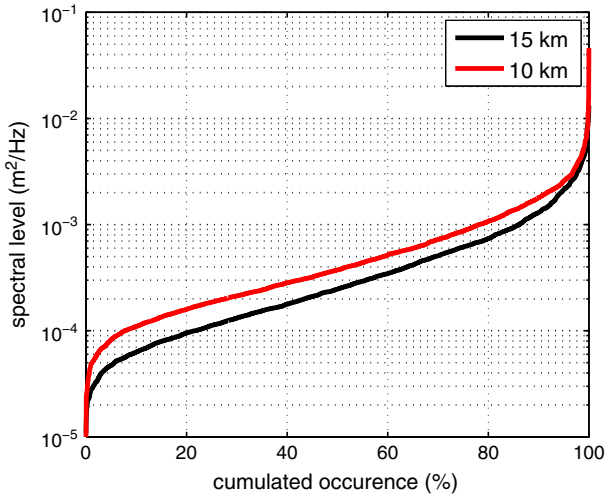

Figure 4. Cumulated occurrence of the spectral level of the surface elevation spectrum $E(f)$ at the DART station 46405, for frequencies 0.0097 and 0.0123 Hz, corresponding to wavelengths of 15 and 10 km, respectively. For 3600 m depth and isotropic spectra, 0.002 m^2/Hz corresponds to an along-track spectral level of 1 cm^2/(cycle/km) at a wavelength of 15 km.

[16] At the site of the 46405 DART station, this level is exceeded 6% of the time (Figure 4), and a level 10 times lower is exceeded more than half of the time. This demonstrates that free IG waves cannot be ignored in the error budget for the future SWOT mission, alongside internal tides [e.g., *Arbic et al.*, 2010]. In particular, the frequency spectral level generally increases at least for frequencies up to 0.015 Hz, suggesting that the free infragravity waves may dominate sea level signals at a scale somewhere between 1 and 10 km.

5. Conclusions

[17] Our analysis of 40 bottom pressure records with multi-year time series clearly reveals a strong seasonal cycle of infragravity (IG) noise levels and energies much higher than previously reported, with a shown increase from West to East in the Pacific Ocean, consistent with higher incident wave heights on the eastern shores of the basins. While we suspect, this West to East increase also exists in the Atlantic, a lack of available data in the NE Atlantic prevents us from showing it.

[18] At one of these location, off the U.S. West coast in 3600 m depth, the mean IG wave height reaches 1.5 cm. There, at a wavelength of 15 km, the along-track spectral level $E(k_x) = 1$ cm^2/(cycle/km) is reached 6% of the time, which was the initial target level for the total error in sea level measurements expected from Surface Water Ocean Topography. Hence, free IG waves cannot be ignored in future high-resolution altimetric measurements in the deep

ocean. At present, there is no known method to correct altimeter data for IG waves contamination because the phase of the waves is random. At best, it should be possible to determine the magnitude of the contamination by estimating the spectrum of free IG waves from the release of bound IG waves at the shoreline. A numerical model based on this idea is now under development. In coastal areas, IG waves will have even higher amplitudes but shorter wavelengths. Further studies will thus be needed to determine the possible impact of IG waves on coastal altimetry measurements.

[19] **Acknowledgments.** Bottom pressure data were provided by the U.S. National Ocean Data Center, V. Ballu (IPGP) and the Australian Bureau of Meteorology. F.A. is funded by ERC grant #240009 "IOWAGA" with additional support from the U.S. National Ocean Partnership Program, under grant N00014-10-1-0383 and Labex Mer via grant ANR-10-LABX-19-01. This particular effort on infragravity waves is supported by the French "Investissements d'avenir" through CNES and the SWOT preparation program. This manuscript was partly written when author JA was hosted by Mark Merrifield and Douglas Luther at the University of Hawaii Sea Level Center.

References

Alsdorf, D., L.-L. Fu, N. Mognard, A. Cazenave, E. Rodriguez, D. Chelton, and D. Lettenmaier (2007), Measuring global oceans and terrestrial freshwater from space, *Eos*, *88*(24), 253–257.

Arbic, B. K., A. J. Wallcraft, and E. J. Metzger (2010), Concurrent simulation of the eddying general circulation and tides in a global ocean model, *Ocean Modell.*, *32*, 175–187.

Ardhuin, F., and T. H. C. Herbers (2013), Double-frequencynoise generation by surface gravity waves in finite depth: Gravity, acoustic and seismic modes, *J. Fluid Mech.*, *716*, 316–348.

Bromirski, P. D., O. V. Sergienko, and D. R. MacAyeal (2010), Transoceanic infragravity waves impacting Antarctic ice shelves, *Geophys. Res. Lett.*, *37*, L02502, doi:10.1029/2009GL041488.

de Jong, M. P. C., L. H. Holthuijsen, and J. A. Battjes (2003), Generation of seiches by cold fronts over the southern north sea, *J. Geophys. Res.*, *108*(C4), 3117, doi:10.1029/2002JC001422.

de Laplace, P. S. (1776), Suitedes recherches sur plusieurs points du système du monde (XXV–XXVII), *Mém. Présentés Acad. R. Sci. Inst. France*, 542–552.

Filloux, J. H. (1980), Pressure fluctuations on the open ocean floor over a broad frequency range: New program and early results, *J. Phys. Oceanogr.*, *10*(12), 1959–1971.

Filloux, J. H., D. Luther, and A. Chave (1991), Long-term seafloor measurement of water pressure: Normal modes and infragravity waves, in *Proceedings of the XXth General Assembly IUGG*, Vienna, Austria.

Harmon, N., T. Henstock, M. Srokosz, F. Tilmann, A. Rietbrock, and P. Barton (2012), Infragravity wave source regions determined from ambient noise correlation, *Geophys. Res. Lett.*, *39*, L04604, doi: 10.1029/2011GL050414.

Henderson, S. M., and A. J. Bowen (2003), Observations of surf beat forcing and dissipation, *J. Geophys. Res.*, *107* (C11), 3193, doi: 10.1029/2000JC000498.

Herbers, T. H. C., S. Elgar, and R. T. Guza (1994), Infragravity-frequency (0.005-0.05 Hz) motions on the shelf. Part I: Forced waves, *J. Phys. Oceanogr.*, *24*, 917–927.

Herbers, T. H. C., S. Elgar, and R. T. Guza (1995), Infragravity-frequency (0.005-0.05 Hz) motions on the shelf. Part II: Free waves, *J. Phys. Oceanogr.*, *25*, 1063–1079.

Luther, D. S., A. D. Chave, J. H. Filloux, and P. F. Spain (1990), Evidence for local and nonlocal barotropic responses to atmospheric forcing during BEMPEX, *Geophys. Res. Lett.*, *17*(7), 949–952.

Le Traon, P. Y. L., P. Klein, B. L. Hua, and G. Dibarboure (2008), Do altimeter wavenumber spectra agree with the interior or surface quasigeostrophic theory? *J. Phys. Oceanogr.*, *38*, 1137–1142.

Webb, S., X. Zhang, and W. Crawford (1991), Infragravity waves in the deep ocean, *J. Geophys. Res.*, *96*, 2723–2736.

Webb, S. C. (2008), The earth's hum: The excitation of earth normal modes by ocean waves, *Geophys. J. Int.*, *174*(2), 542–566, doi:10.1111/j.1365-246X.2008.03801.X.

Xu, Y., and L.-L. Fu (2011), Global variability of the wavenumber spectrum of oceanic mesoscale turbulence, *J. Phys. Oceanogr.*, *41*, 802–809.